NASA TECHNICAL NOTE

NASA TN D-5791

NASA TN D-5791

WEDGE-INDUCED LAMINAR-BOUNDARY-LAYER SEPARATION ON A FLAT PLATE IN LOW-DENSITY, HYPERVELOCITY FLOW

by John B. Anders

Langley Research Center
Hampton, Va. 23365

NATIONAL AERONAUTICS AND SPACE ADMINISTRATION • WASHINGTON, D. C. • APRIL 1970

1. Report No. NASA TN D-5791	2. Government Accession No.	3. Recipient's Catalog No.
4. Title and Subtitle WEDGE-INDUCED LAMINAR-BOUNDARY-LAYER SEPARATION ON A FLAT PLATE IN LOW-DENSITY, HYPERVELOCITY FLOW		5. Report Date April 1970 6. Performing Organization Code
7. Author(s) John B. Anders		8. Performing Organization Report No. L-6847
9. Performing Organization Name and Address NASA Langley Research Center Hampton, Va. 23365		10. Work Unit No. 129-01-22-13-23 11. Contract or Grant No.
12. Sponsoring Agency Name and Address National Aeronautics and Space Administration Washington, D.C. 20546		13. Type of Report and Period Covered Technical Note 14. Sponsoring Agency Code
15. Supplementary Notes		

16. Abstract

An experimental investigation has been made of high-temperature, low-density, hypersonic, laminar-boundary-layer separation on a flat plate with a trailing-edge flap. Both blunt- and sharp-leading-edge models were tested at a free-stream Mach number of 14.5, a free-stream Reynolds number of 2.5×10^4 per foot (8.2×10^4 per meter), and a stagnation enthalpy of 2000 Btu/lbm (4.65 MJ/kg).

In comparison with other higher density, laminar-separation data, boundary-layer separation was delayed on the sharp-leading-edge model at the low-density conditions of the present tests. Calculations indicated that merged-layer flow occurred over most of the model.

Free-interaction parameters correlate the blunt-leading-edge plateau-pressure data with other high Mach number data. Viscous hypersonic similitude parameters correlate both blunt and sharp data and indicate that the plateau pressure depends primarily on the viscous interaction parameter and weakly on nose bluntness.

17. Key Words (Suggested by Author(s)) Laminar boundary layer Separation Low density	18. Distribution Statement Unclassified – Unlimited		
19. Security Classif. (of this report) Unclassified	20. Security Classif. (of this page) Unclassified	21. No. of Pages 29	22. Price* $3.00

*For sale by the Clearinghouse for Federal Scientific and Technical Information
Springfield, Virginia 22151

WEDGE-INDUCED LAMINAR-BOUNDARY-LAYER SEPARATION ON A FLAT PLATE IN LOW-DENSITY, HYPERVELOCITY FLOW

By John B. Anders
Langley Research Center

SUMMARY

An experimental investigation has been made of high-temperature, low-density, hypersonic, laminar-boundary-layer separation on a flat plate with a trailing-edge flap. Both blunt- and sharp-leading-edge models were tested at a free-stream Mach number of 14.5, a free-stream Reynolds number of 2.5×10^4 per foot (8.2×10^4 per meter), and a stagnation enthalpy of 2000 Btu/lbm (4.65 MJ/kg).

Oil flow patterns indicated regions of three-dimensional flow on the model. Addition of full-length end plates resulted in a more two-dimensional flow on the model surface.

In comparison with other higher density, laminar-separation data, boundary-layer separation was delayed on the sharp-leading-edge model at the low-density conditions of the present tests. Calculations indicated that merged-layer flow occurred over most of the model.

Free-interaction parameters correlate the blunt-leading-edge plateau-pressure data with other high Mach number data. Viscous hypersonic similitude parameters correlate both blunt and sharp data and indicate that the plateau pressure depends primarily on the viscous interaction parameter and weakly on nose bluntness.

INTRODUCTION

Boundary-layer separation ahead of control surfaces continues to be a problem only partially predictable by present theoretical means. Entry vehicles with separation ahead of control surfaces might obtain important changes in aerodynamic characteristics because of large center-of-pressure shifts and higher local heating rates on certain areas of the vehicle. These problems have an added degree of uncertainty when the flight regime includes low-density, high-temperature, hypersonic flow where the fluid behavior departs from that of a perfect gas. Heating rates in such a regime can easily exceed design limitations when reattachment occurs on the control surface.

In order to avoid an excessive weight penalty from an elaborate thermal protection system, it is desirable to know when, or whether, separation occurs on a reentry vehicle utilizing flap-type controls and flying at hypersonic speeds at high altitudes. Although theoretical methods have been unable to predict low-density separation of a real gas, experimental data have provided a few of the details of such a flow (refs. 1 to 5). However many questions remain unanswered. For example, at high altitudes the boundary layer begins to merge with the bow shock, and the inviscid region between the edge of the boundary layer and the shock wave disappears. The question is whether, under such conditions, the boundary layer separates ahead of a deflected control or simply swallows the obstruction. Other questions involve the effects of real gases, slip flow at the wall, leading-edge thickness, and the existence of free interaction.

The present investigation attempts to answer some of these questions.

SYMBOLS

$C^* = \dfrac{\mu^* T_\infty}{\mu_\infty T^*}$

$c_{f,o}$ local skin-friction coefficient at beginning of interaction

$C_{p,p}$ plateau-pressure coefficient

H stagnation enthalpy

k nose drag coefficient

$K_{\epsilon,o}$ nose bluntness parameter, $\epsilon M_o^3 k(t/x)$

L plate length from nose to hinge line

M Mach number

p pressure

R gas constant

$R_{o,s}$ local Reynolds number at beginning of interaction based on surface distance s

R_∞ free-stream unit Reynolds number

$R_{\infty,L}$ free-stream Reynolds number based on total plate length

s surface distance down model

t leading-edge thickness

T temperature

T_{std} temperature at standard conditions, 491.69° R (273.16° K)

T^* reference temperature, $\frac{T_t}{6}\left(1 + 3\frac{T_w}{T_t}\right)$

$\overline{V}_{\infty,L}$ rarefaction parameter, $M_\infty\sqrt{C^*/R_{\infty,L}}$

x longitudinal coordinate

$\beta_o = \sqrt{M_o^2 - 1}$

γ ratio of specific heats

$\epsilon = (\gamma - 1)/(\gamma + 1)$

θ flap deflection angle

μ coefficient of viscosity

μ^* coefficient of viscosity evaluated at reference temperature T^*

$\overline{\chi}_{\infty,s}$ viscous interaction parameter, $M_\infty^3\sqrt{C^*/R_{\infty,s}}$

$\overline{\chi}_{\epsilon,o} = \epsilon\left(0.664 + 1.73\frac{T_w}{T_t}\right)\overline{\chi}_{\infty,s}$

Subscripts:

aw adiabatic wall

o beginning of interaction

p	plateau region
t	stagnation condition
w	model wall
∞	free stream

APPARATUS AND TESTS

Test Facility

Tests were conducted in the Langley 1-foot (0.305-meter) hypersonic arc tunnel, which uses electric-arc-heated air at a stagnation pressure of about 20 atm (1 atm = 101 kN/m^2) as the test medium. The air expands down a 5^o half-angle conical nozzle to a 1-foot-diameter (0.305-m) test section where the nominal free-stream Mach number is 14.5 and the nominal free-stream Reynolds number is 2.5×10^4 per foot (8.2×10^4 per meter). A detailed description of the facility is presented in reference 6.

Model

The model used in the present tests was a water-cooled flat plate with a trailing-edge flap. The plate had a span of 4 inches (10.16 cm) and a chord of 5.5 inches (13.97 cm) with interchangeable blunt and sharp leading edges. The hemicylindrically blunt leading edge had a radius of 0.125 inch (0.317 cm) and the sharp leading edge had a diameter of approximately 0.002 inch (0.0051 cm) with a 20^o bevel angle on its lower surface. Flap angles were variable from 0^o to 45^o; however, tunnel blockage influenced the flow at flap angles greater than 37^o. The model was fitted with two interchangeable sets of end plates. The smaller set enclosed only a small region near the model flap hinge line and the larger set extended the length of the model as shown in figure 1. A photograph of the model with the blunt leading edge and the large end plates is shown in figure 2.

Instrumentation

Model instrumentation consisted of eighteen 0.060-inch-diameter (0.152-cm) pressure orifices and seven chromel-alumel thermocouples. The inside diameter of all pressure tubing was increased to 0.090 inch (0.229 cm) inside the model to reduce the pressure lag. The pressure tubing connected to ionization-type pressure sensors, and both the thermocouple and ionization-gage outputs were monitored continuously on oscillograph film recorders. Model instrumentation locations are shown in figure 3.

Test Conditions and Data Accuracy

The stagnation enthalpy, calculated by using the sonic-throat method described in reference 7, was compared extensively with calorimeter measurements in reference 8 and found to be within ±10 percent of the measured value at values of H/RT_{std} less than 74. The stagnation pressure was set as high as possible in order to obtain the maximum free-stream Reynolds number.

Nonequilibrium nozzle calculations coupled with experimental measurements were used to determine the flow properties in the tunnel test section. Vibrational nonequilibrium in the nozzle was accounted for by using relaxation rates determined from electron-beam measurements of the vibrational temperature in the test section (ref. 9). These measurements indicated that the vibrational temperature was frozen a short distance downstream of the throat. All chemical reactions were assumed frozen in the stagnation chamber.

The mean free path in the test-section free stream was approximately 0.015 inch (0.038 cm). Thus, the Knudsen number was approximately 7.0 based on the sharp-leading-edge thickness.

Table I shows the nominal tunnel conditions for the tests. The plate was set at zero angle of attack for all tests and the flap angle varied from 32° to 37°. The ratio of model-wall to stagnation temperature T_w/T_t was approximately 0.10.

The maximum possible error in pressure measurement was ±5 percent. In addition, the data were subject to an uncorrected error of -6 percent maximum due to an orifice effect (refs. 4 and 10).

Test Methods

Pressure tubing from the model was connected to pressure transducers through remotely controlled valves. In order to minimize contamination from the stream, the gages were pressurized with dry air to a level higher than the expected measurement just prior to a test. The tunnel was started and allowed to reach a steady condition (approximately 15 seconds) whereupon the remotely controlled valves were opened and the gage pressures allowed to decrease to a steady value. The pressures were continually recorded on oscillograph tape during this steadying process which usually required 2.5 to 3 minutes. When the traces showed a negligible change with time, the valves were closed and a pitot probe was inserted into the stream to a point 1 inch (2.54 cm) below the tunnel center line and 1/4 inch (0.635 cm) upstream of the model nose. The probe was connected to a pressure transducer through a remotely controlled valve similarly to the model surface orifices. The probe gage was pressurized to approximately 27.85 lb/ft^2 (1333 N/m^2), and when the valve was opened, the pressure was observed

to decrease to a steady value in about 5 seconds. The reading of the probe was continuously recorded on the oscillograph tape, and when a steady value was reached, the valve was closed and the run terminated. All gages were then evacuated and kept under vacuum until the next test. The stagnation enthalpy was determined from measurements made at the end of the test to minimize any error due to enthalpy change with time.

The oil flow tests were not made simultaneously with the pressure tests since the oil patterns became very faint in the length of time required for the pressures to reach a steady value. Consequently, each oil flow pattern was obtained during a separate test with the same model geometry.

Prior to an oil pattern test the model was cleaned and dotted with small drops of diffusion-pump oil tinted with Prussian blue pigment. The tunnel startup procedure was altered in order to expose the model to the airstream a minimum length of time before the arc fired. This startup time usually took from 2 to 3 seconds and the oil pattern showed negligible change during this time. As soon as the arc was fired, the oil dots began to move and reached a steady position in approximately 20 seconds. The tunnel was then shut down with no noticeable change in the pattern occurring during the shutdown procedure. The model was removed from the test section, photographed, cleaned, and reinstalled for the next test.

RESULTS AND DISCUSSION

Three-Dimensional Effects

The flat-plate model used in the present tests had an aspect ratio of approximately 0.70. Although a larger aspect ratio was desirable, the span of the model could not be increased beyond 4 inches (10.16 cm) because of tunnel blockage. End plates were used to restrict the spanwise flow of fluid on the model and oil flow tests were made to determine the edge effects.

Figure 4 shows typical oil flow patterns for both sharp- and blunt-leading-edge models. Two sizes of end plates were tested and results from both are shown in figure 4 as well as the case with no end plates.

The streamlines on the model without end plates indicate a lateral flow of fluid on the plate and on the flap. Very little separation is present on either the blunt or the sharp plate. The addition of small end plates reduces the divergence of the streamlines on the aft portion of the plate but does little to improve the flow over the forward portion. The flow on the sharp plate appears to be considerably more parallel than that on the blunt plate. The flow over the flap for both sharp and blunt leading edges still shows strong edge effects, particularly near the trailing-edge corners. Separation appears to have

moved forward, especially near the model—end-plate junction where a curved line of separation is formed.

The large end plates eliminate the edge venting effect. Both the blunt- and sharp-leading-edge models show the outboard streamlines curving in on the rearward portion of the model; however, the central portion shows fairly uniform flow. The flap still shows three-dimensional flow in spite of the end plates.

The addition of the end plates has apparently affected the flow over the model in two ways: First, the end plates limit the spanwise venting of air from the central region of the model and thus allow the separation bubble to grow larger. Second, the end plates create a corner flow in the area near the model—end-plate junction. The flowing gas in this corner has lower momentum, and consequently, with the flap deflected the flow separates from the model surfaces sooner than at midspan. The higher pressure separated fluid in the corners then forces nearby streamlines in toward the lower pressure unseparated flow in midspan.

Figure 5 shows the effect of the end plates on the measured pressure distributions. The beginning of interaction moves forward for both blunt- and sharp-leading-edge models as the end-plate size increases. For the blunt-leading-edge model, the plateau level changes from an inflection point to a well-defined plateau as the end-plate size increases. The changes for the sharp-leading-edge model are not as large, but the inflection point does broaden and approach a constant-pressure plateau.

The outboard pressures shown in figure 5 are from locations 1 inch (2.54 cm) on either side of the model center line. The difference between the center and outboard pressures was a maximum of 20 percent. Since the outboard orifices were located in the initial interaction region where the pressure was rapidly changing from the undisturbed level to the plateau level, slight variations in the extent of separation in the spanwise direction could easily cause an appreciable difference between the center and outboard measurements. Close examination of the pressure distribution and oil flow patterns in figures 4 and 5 indicates that a spanwise change in the separation point of the order of $\Delta x/L = 0.035$ would result in a spanwise pressure variation of 20 percent.

In summary, three-dimensional flow existed on the present model, both on the flap and on the plate. However, oil flow patterns indicate that with the large end plates on the model, the central region of the plate experienced essentially two-dimensional flow. The large end plates eliminated the edge venting effect on the plate and increased the size of the separation bubble. The flow over the flap showed spanwise variations that were not eliminated by the addition of end plates.

Flap-Chord Effects

The present tests were conducted at low Reynolds numbers with correspondingly thick boundary layers. The boundary-layer thickness at the hinge line for an unseparated flow over the present model was calculated by the method of reference 11 to be approximately 0.7 inch (1.78 cm). A boundary layer of this thickness approaches the height of the flap above the model surface. Even at the highest flap angle tested the boundary-layer thickness at the model hinge line was 78 percent of the flap height. The total length of the flap was approximately twice the boundary-layer thickness. A chord extension plate that lengthened the flap by 33 percent was installed but resulted in tunnel blockage problems and thus could not be used. The measured peak pressures on the basic flap with the blunt-leading-edge model were as much as 10 percent lower than the calculated inviscid wedge pressure. This indicates that the flow upstream was being influenced by the flap trailing edge. Oil flow patterns indicated that reattachment, at its most downstream location, occurred at approximately 57 percent of the flap chord.

Pressure Distributions

Figure 6 shows typical pressure distributions at various flap angles for both blunt and sharp leading edges. At the lowest flap angle, separation is not well developed; that is, there is no constant-pressure plateau region. As the flap angle increases, the beginning of interaction moves forward and the plateau region becomes more evident. References 1 and 2 show examples of what Album (ref. 1) terms "partially developed" separation; that is, the plateau region reduces to an inflection point. As the size of the separation region increases (increasing flap angle here), the region changes to the "well-developed" state. Reference 2 suggests that the lack of a plateau in partially developed separation is a result of the upstream influence of the reattachment process. The results in reference 2 were for separation ahead of forward-facing steps, and pressure plateaus were found only for large step heights.

The sharp-leading-edge pressure distributions shown in figure 6(b) indicate that the boundary layer was separated but did not reach the well-developed state in the range of conditions studied. Oil flow studies confirm this result. The rarefaction parameter $\overline{V}_{\infty,L}$ is quite high for these tests, about 0.15. Reference 12 indicates that for a rarefaction parameter of approximately 0.16, the flow over a flat plate is in the merged-flow regime with slip flow at the wall and a greatly thickened viscous layer extending to the shock wave. Certainly a portion of the present model experienced this type of flow, and quite possibly slip flow at the wall occurred over the entire length of the plate.

If slip flow does occur, the velocity profile near the wall is slightly fuller and the fluid has correspondingly higher momentum and, as a result, penetrates farther into the adverse pressure gradient generated by the deflected flap. The thick viscous layer has

the effect of reducing the effectiveness of the flap by "smoothing" over any obstruction to the flow. It is reasonable, then, to find less separation on the sharp-leading-edge plate at these conditions than at higher density conditions. In fact, the size of the separation bubble appears to be reduced to a scale comparable with the blunt-leading-edge results. Reference 4 indicated no separation on a sharp plate at flap angles as high as 35° where $\overline{V}_{\infty,L}$ was approximately 0.20 for a model chord of 2.5 inches (6.4 cm). For the present tests, the chord was almost twice that of reference 4.

Extent of Separation

Separation lengths were obtained from the oil flow patterns, and figure 7 shows the variation of the separation and reattachment points as well as the bubble length with flap angle. The points are not exactly defined by the oil flow patterns and are represented by a band within which separation or reattachment could occur.

The separation point for both the blunt and sharp leading edges moved nearly linearly upstream with increasing flap angle.

The reattachment points for the sharp-leading-edge tests generally occur slightly downstream of the blunt-leading-edge results, as shown in figure 7. The net result is that the bubble length is slightly longer for the sharp leading edge than for the blunt leading edge. Again, it must be noted that the differences between the sharp and blunt results are small and the conclusions are subject to the interpretation of the oil flow photographs.

Plateau Pressure Correlations

Since there are several correlation forms for the plateau pressure available in the literature, the present data have been applied to three of these correlations in order to test their validity with respect to low-density, high-temperature data. Perhaps the most familiar of these correlations is that presented in reference 13. This correlation, shown in figure 8, is usually considered valid for flat plates at low supersonic Mach numbers with moderate boundary-layer cooling; however, in the present high Mach number, highly cooled case, it graphically shows the relationship of the present data to data from references 3, 4, 13, and 16 to 21. Although almost two orders of magnitude lower in Reynolds number than most previous data, the present blunt-leading-edge results show fair agreement with linear theory (shown as the solid line). Previous low-density data obtained in the same facility as the present data show similar agreement. The present sharp-leading-edge results also show fair agreement with linear theory, in spite of the fact that separation was not completely developed and the plateau pressure was estimated from the inflections in the pressure distributions.

The same correlation in a slightly different form is shown in figure 9, which is from reference 14. The skin-friction coefficient for use with the present data was calculated by

the method of reference 11. An average of measured wall temperature was used. This correlation of high Mach number data is somewhat better than that in figure 8 and the present blunt-leading-edge results are in closer agreement with other data (refs. 13, 18 to 20, 22, and 23).

Since the correlation of figure 9, or its more restrictive form in figure 8, was developed from the principle of free interaction, agreement with this correlation implies that free interaction does exist. The term "free interaction" means that the interaction of the inviscid flow with the viscous flow depends only on conditions at the beginning of the interaction. This is obviously true in figure 9 since data for wedge, step, and curved corners all correlate reasonably well and thus indicate that the downstream geometry is unimportant. Reference 1 empirically extended the principle of free interaction to the case of separation of a thick, slightly rarefied boundary layer with upstream tip bluntness effects. The present blunt-leading-edge data offer some confirmation of this extension with considerably larger bluntnesses.

Figure 10 shows a somewhat different type of correlation utilizing viscous, hypersonic similitude parameters from reference 15 as suggested by Holden (ref. 5). The present data correlate well and the sharp-leading-edge data extend the correlation almost two orders of magnitude below the data of reference 5. The slope of the faired line in figure 10 is very nearly -3 (the actual value is -2.87). Using the approximate value of -3 and writing the equation of the line yields values of p_p/p_o independent of nose bluntness, but which are a linear function of $\overline{\chi}_{\epsilon,o}$. The parameter p_p/p_o when plotted against $\overline{\chi}_{\epsilon,o}$ shows large scatter and thus indicates that the bluntness parameter is more important than the slight deviation of the power from the value -3 would indicate. Figure 11 shows the results of using the actual value of the slope and writing the equation of the line shown in figure 10. The bluntness parameter appears to a small power; and the viscous interaction parameter, to a power slightly larger than unity. From figure 11 it is clear that nose bluntness has a small but significant role on the plateau pressure.

CONCLUSIONS

An investigation has been made of the separation of a high-temperature, low-density, hypersonic, laminar boundary layer on a flat plate with a trailing-edge flap. Tests were made to determine the pressure distributions and the size of the interaction region on the plate for both blunt and sharp leading edges. The results of the investigation indicate the following:

1. The addition of full-length end plates on the model significantly increased the size of the interaction region. Oil flow patterns indicated nearly two-dimensional flow in the central region of the flat plate with full-length end plates attached. The flow over the trailing-edge flap was three-dimensional both with and without end plates.

2. In relation to laminar-separation data in the literature at higher density, boundary-layer separation was delayed on the sharp-leading-edge flat plate at the low-density conditions of the present tests. Values of the rarefaction parameter indicate that the flow over the plate is in the merged-layer regime with slip flow at the wall. The size of the separation bubble for both blunt and sharp leading edges is comparable even though for the blunt case the local Mach number was approximately 3.5 and the local Reynolds number was about 1.5 percent of the sharp-case value.

3. The measured plateau pressures for the blunt-leading-edge plate correlated using linear free-interaction-theory parameters. The correlation implies the existence of free interaction at the low-density conditions encountered in the present tests.

4. Viscous hypersonic similitude parameters correlate plateau pressure data for both blunt- and sharp-leading edge models and indicate that the plateau pressure depends primarily on the viscous interaction parameter and weakly on nose bluntness.

Langley Research Center,
National Aeronautics and Space Administration,
Langley Station, Hampton, Va., February 20, 1970.

REFERENCES

1. Album, Harvey H.: Hypersonic Laminar Separation in Minutely Blunted Cones in Slip Flow. AFOSR 67-1507, U.S. Air Force, May 1967. (Available from DDC as AD 663475.)

2. Rogers, E. W. E.; Berry, C. J.; and Davis, B. M.: An Experimental Investigation of the Interaction Between a Forward-Facing Step and a Laminar Boundary Layer in Supersonic, Low-Density Flow. R. & M. No. 3506, Brit. A.R.C., 1967.

3. Anders, John B.; and Edwards, C. L. W.: A Real-Gas Study of Low-Density Wedge-Induced Laminar Separation on a Highly Cooled Blunt Flat Plate at $M_\infty = 12$. NASA TN D-4320, 1968.

4. Edwards, C. L. W.; and Anders, John B.: Low-Density, Leading-Edge Bluntness, and Ablation Effects on Wedge-Induced Laminar-Boundary-Layer Separation at Moderate Enthalpies in Hypersonic Flow. NASA TN D-4829, 1968.

5. Holden, Michael S.: Leading-Edge Bluntness and Boundary-Layer Displacement Effects on Attached and Separated Laminar Boundary Layers in a Compression Corner. AIAA Pap. No. 68-68, Jan. 1968.

6. Boatright, W. B.; Stewart, R. B.; and Sebacher, D. I.: Testing Experience and Calibration Experiments in a Mach Number 12, 1-Foot Hypersonic Arc Tunnel. Third Hypervelocity Techniques Symposium, Univ. of Denver and Arnold Eng. Develop. Center, Mar. 1964, pp. 182-212.

7. Jorgensen, Leland H.: The Total Enthalpy of a One-Dimensional Nozzle Flow With Various Gases. NASA TN D-2233, 1964.

8. Boatright, W. B.; Sebacher, D. I.; Guy, R. W.; and Duckett, R. J.: Review of Testing Techniques and Flow Calibration Results for Hypersonic Arc Tunnels. AIAA Pap. No. 68-379, Apr. 1968.

9. Sebacher, Daniel I.: A Correlation of N_2 Vibrational → Translational Relaxation Times. AIAA J., vol. 5, No. 4, Apr. 1967, pp. 819-820.

10. Guy, R. W.; and Winebarger, R. M.: Effect of Orifice Size and Heat-Transfer Rate on Measured Static Pressures in a Low-Density Arc-Heated Wind Tunnel. NASA TN D-3829, 1967.

11. Bertram, Mitchel H.; and Feller, William V.: A Simple Method for Determining Heat Transfer, Skin Friction, and Boundary-Layer Thickness for Hypersonic Laminar Boundary-Layer Flows in a Pressure Gradient. NASA MEMO 5-24-59L, 1959.

12. McCroskey, William J.: An Experimental Model for the Sharp Leading Edge Problem in Rarefied Hypersonic Flow. ARL 66-0101, U.S. Air Force, June 1966. (Available from DDC as AD 641996.)

13. Chapman, Dean R.; Kuehn, Donald M.; and Larson, Howard K.: Investigation of Separated Flows in Supersonic and Subsonic Streams With Emphasis on the Effect of Transition. NACA Rep. 1356, 1958. (Supersedes NACA TN 3869.)

14. Bertram, M. H.; Weinstein, L. M.; Cary, A. M., Jr.; and Arrington, J. P.: Heat Transfer to Wavy Wall in Hypersonic Flow. AIAA J., vol. 5, no. 10, Oct. 1967, pp. 1760-1767.

15. Cheng, H. K.; Hall, J. Gordon; Golian, T. C.; and Hertzberg, A.: Boundary-Layer Displacement and Leading-Edge Bluntness Effects in High-Temperature Hypersonic Flow. J. Aerosp. Sci., vol. 28, no. 5, May 1961, pp. 353-381, 410.

16. Harvey, William D.: Experimental Investigation of Laminar-Flow Separation on a Flat Plate Induced by Deflected Trailing-Edge Flap at Mach 19. NASA TN D-4671, 1968.

17. Johnson, Charles B.: Pressure and Flow-Field Study at Mach Number 8 of Flow Separation on a Flat Plate With Deflected Trailing-Edge Flap. NASA TN D-4308, 1968.

18. Sterrett, James R.; and Emery, James C.: Extension of Boundary-Layer-Separation Criteria to a Mach Number of 6.5 by Utilizing Flat Plates With Forward-Facing Steps. NASA TN D-618, 1960.

19. Hakkinen, R. J.; Greber, I.; Trilling, L.; and Abarbanel, S. S.: The Interaction of an Oblique Shock Wave With A Laminar Boundary Layer. NASA MEMO 2-18-59W, 1959.

20. Miller, D. S.; Hijman, R.; and Childs, M. E.: Mach 8 to 22 Studies of Flow Separations Due to Deflected Control Surfaces. AIAA J., vol. 2, no. 2, Feb. 1964, pp. 312-321.

21. Putnam, Lawrence E.: Investigation of Effects of Ramp Span and Deflection Angle on Laminar Boundary-Layer Separation at Mach 10.03. NASA TN D-2833, 1965.

22. Townsend, James C.: Effects of Leading-Edge Bluntness and Ramp Deflection Angle on Laminar Boundary-Layer Separation in Hypersonic Flow. NASA TN D-3290, 1966.

23. Giles, H. L.; and Thomas, J. W.: Analysis of Hypersonic Pressure and Heat Transfer Tests on a Flat Plate With a Flap and a Delta Wing With Body Elevons, Fins, and Rudders. NASA CR-536, 1966.

TABLE I.- NOMINAL TUNNEL TEST CONDITIONS

Quantity	U.S. Customary Units	SI Units
Stagnation pressure	4.95×10^4 lb/ft^2	2.36 MN/m^2
Stagnation enthalpy	2000 Btu/lbm	4.65 MJ/kg
Free-stream Mach number	14.5	14.5
Free-stream Reynolds number	2.5×10^4 per ft	8.2×10^4 per meter
Free-stream pressure	9.1×10^{-2} lb/ft^2	4.36 N/m^2
Mean free path	0.015 inch	0.038 cm

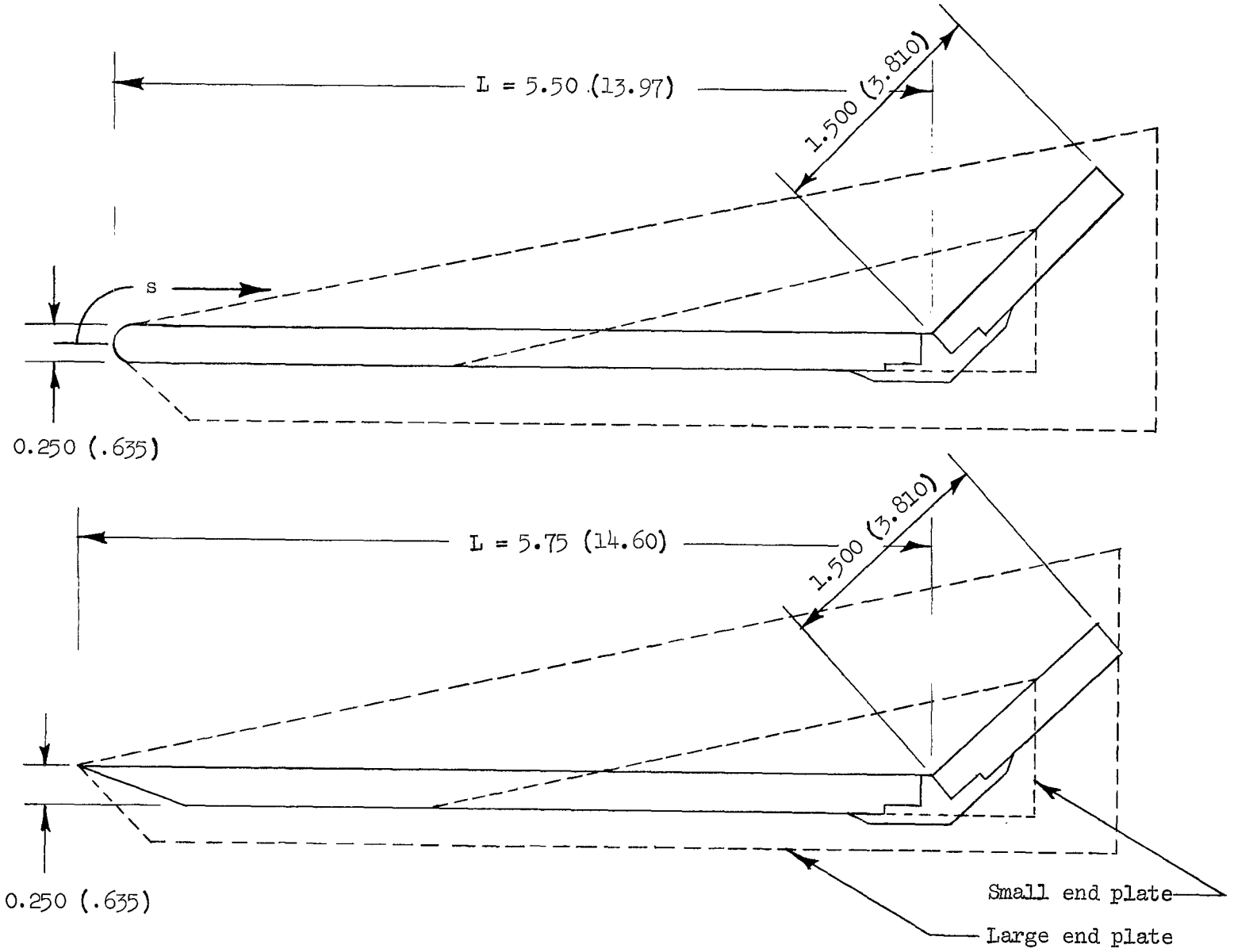

Figure 1.- Blunt- and sharp-leading-edge models showing two sizes of end plates. Dimensions are in inches (cm).

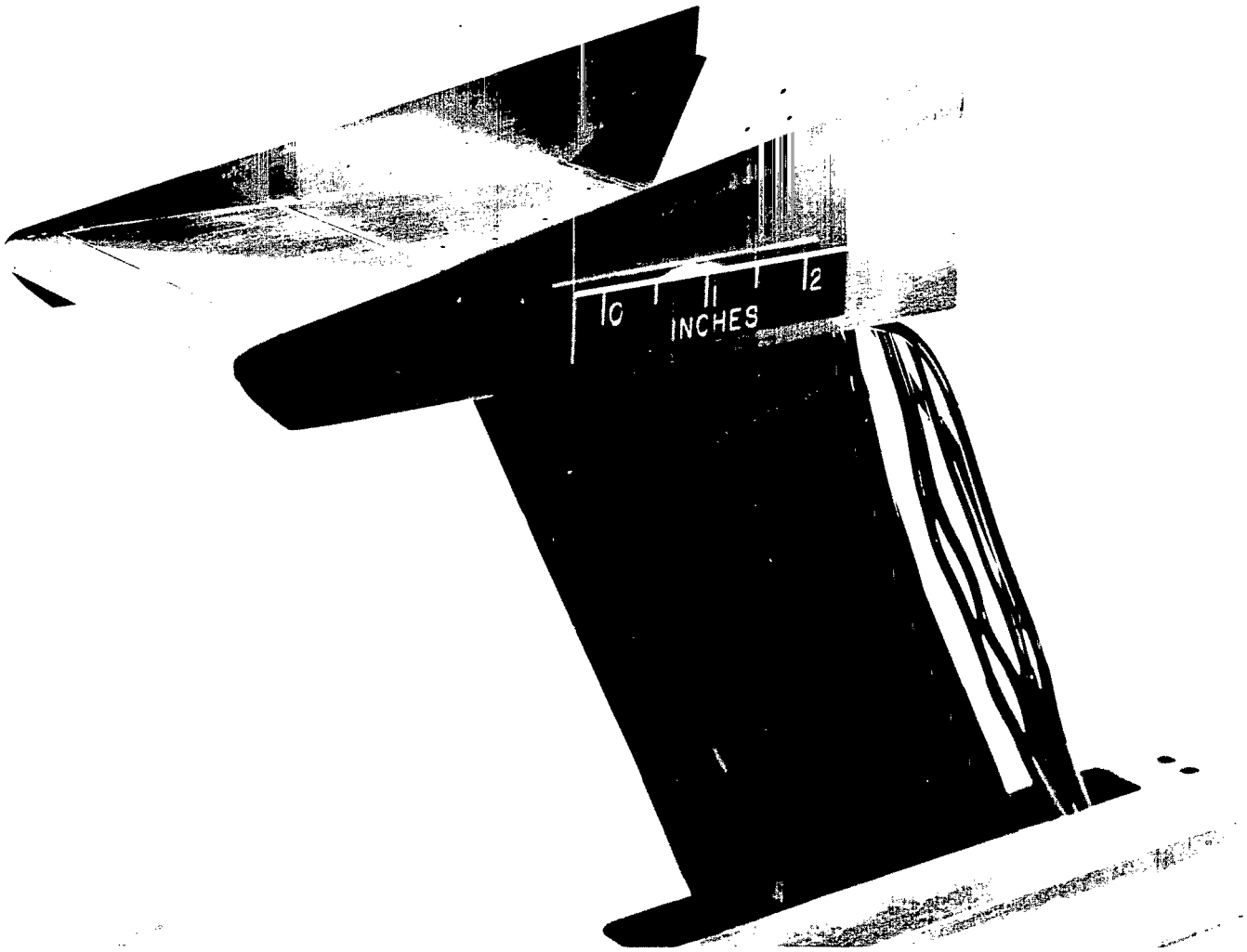

Figure 2.- Photograph of blunt-leading-edge model with large end plates attached. L-69-4172

Pressure Orifices			
Blunt L. E.		Sharp L. E.	
No.	x/L	No.	x/L
1	-0.47	1	-0.46
2	-0.43	2	-0.41
3	-0.38	3	-0.37
4	-0.34	4	-0.33
5	-0.29	5	-0.28
6	-0.24	6	-0.24
7	-0.20	7	-0.19
8	-0.15	8	-0.15
9	-0.11	9	-0.11
10	-0.02	10	-0.02
11	+0.04	11	+0.03
12	+0.09	12	+0.08
13	+0.13	13	+0.12
14	+0.18	14	+0.16
15	+0.22	15	+0.21
16	+0.27	16	+0.25
17	-0.06	17	-0.06
18	-0.11	18	-0.11

Thermocouples			
Blunt L. E.		Sharp L. E.	
No.	x/L	No.	x/L
1	-0.36	1	-0.35
2	-0.27	2	-0.26
3	-0.18	3	-0.17
4	-0.09	4	-0.09
5	+0.06	5	+0.05
6	+0.15	6	+0.14
7	+0.24	7	+0.23

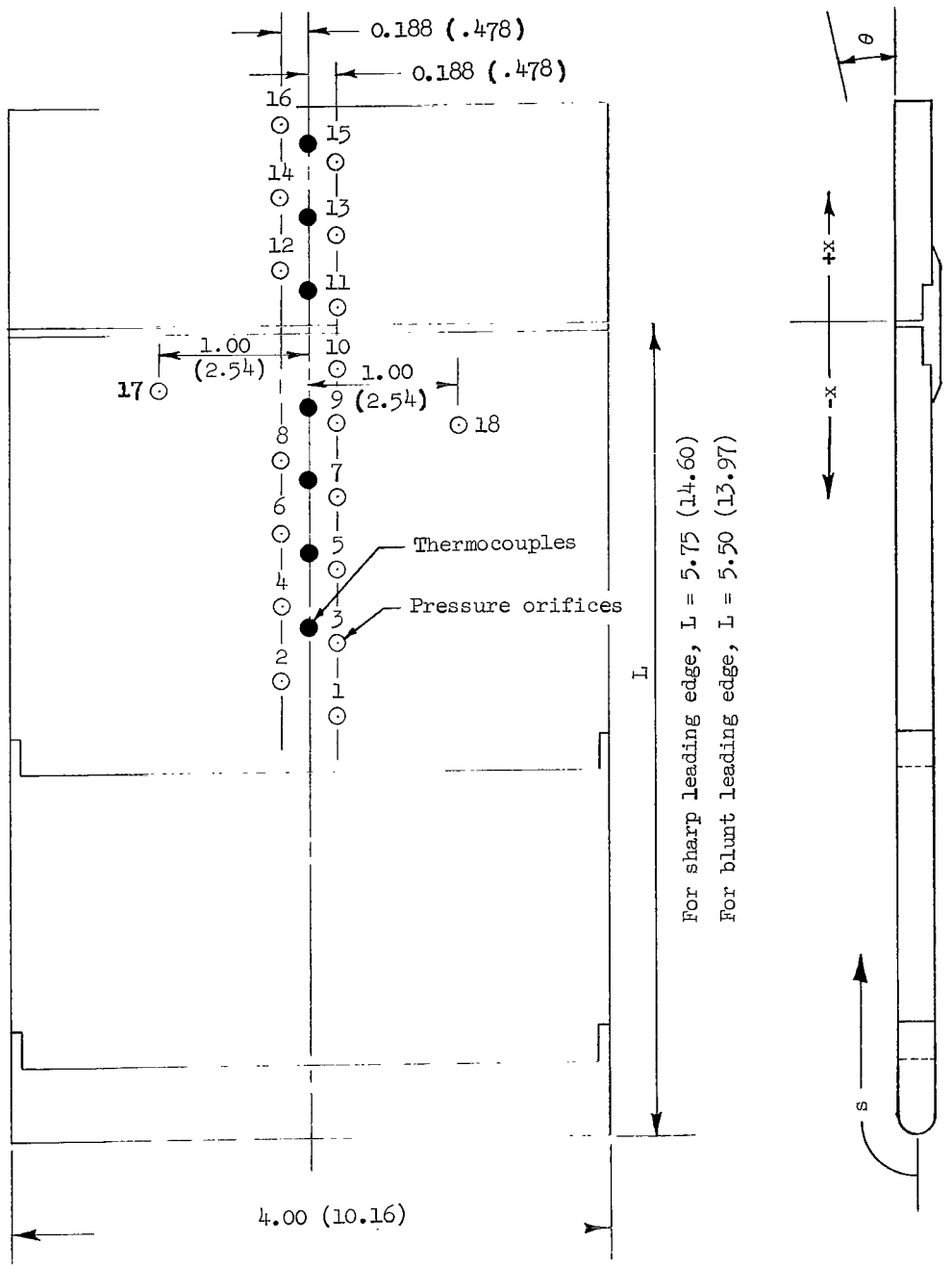

Figure 3.- Model planform and location of instrumentation. Linear dimensions are in inches (cm).

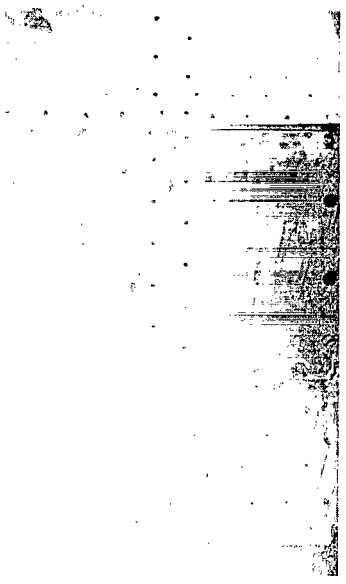

No end plates

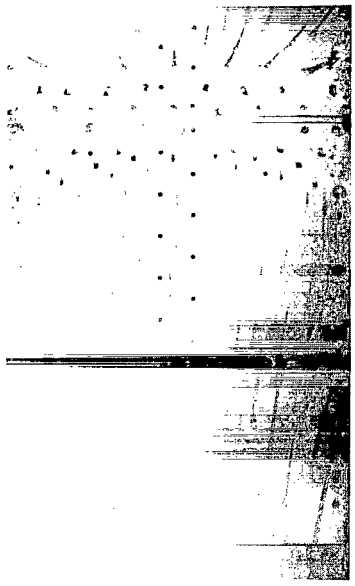

Small end plates

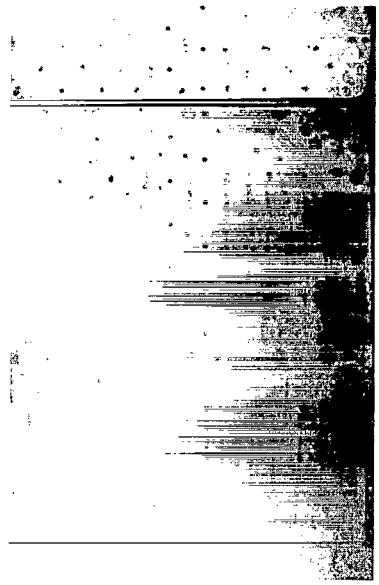

Large end plates

(a) Blunt leading edge.

No end plates

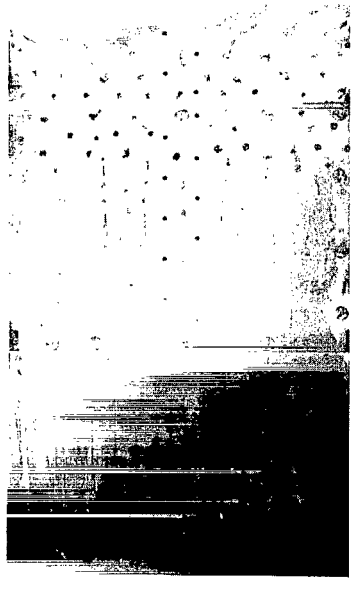

Small end plates

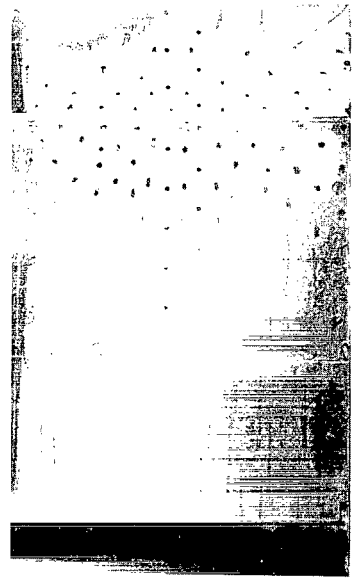

Large end plates

(b) Sharp leading edge.

Figure 4.- Oil flow patterns. $\theta = 37^{o}$; $M_{\infty} = 14.5$; $R_{\infty} = 2.5 \times 10^{4}$ per ft $(8.2 \times 10^{4}$ per m). L-70-1526

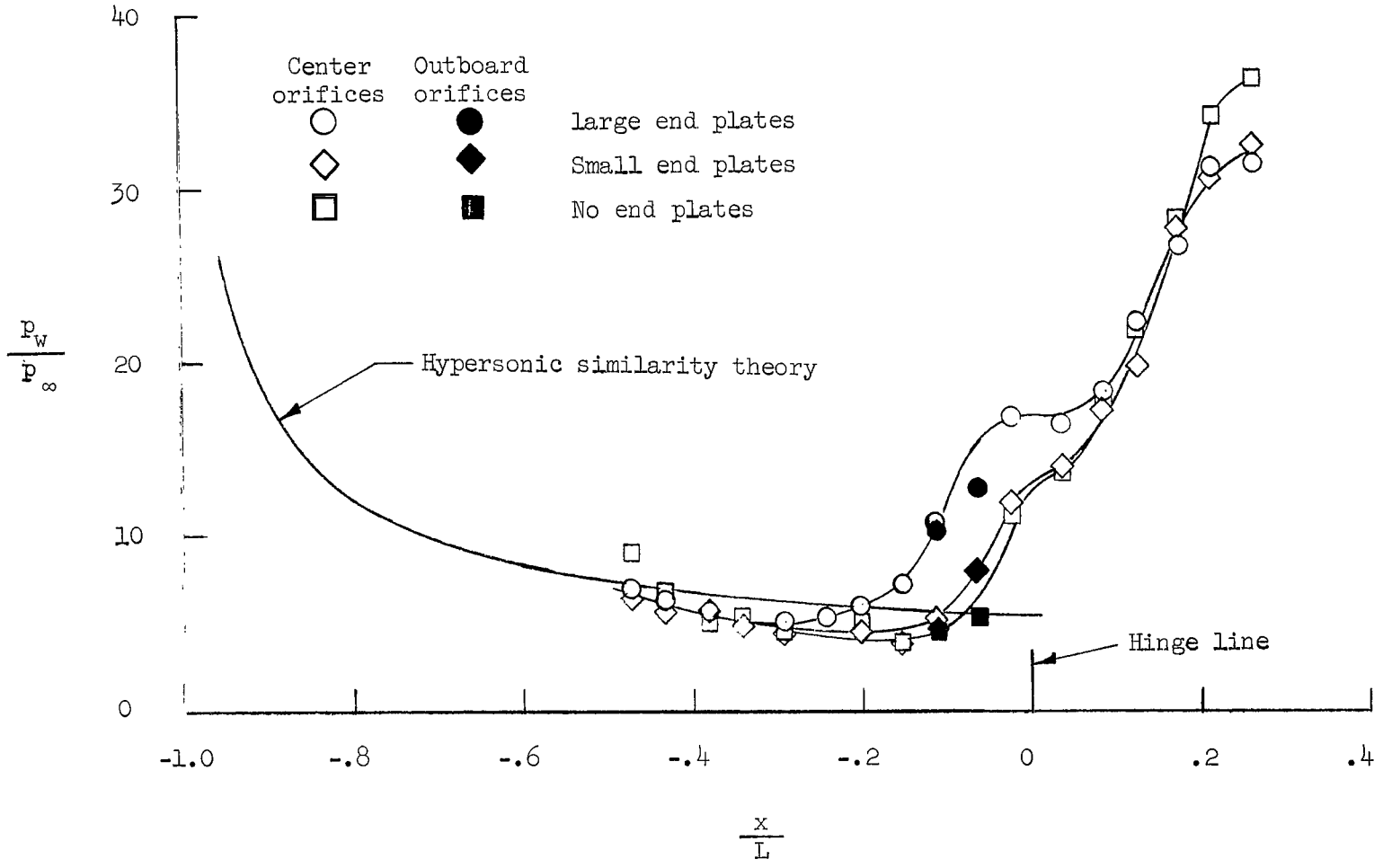

(a) Blunt leading edge.

Figure 5.- Effect of end-plate geometry on pressure distribution. $\theta = 37^0$; $M_\infty = 14.5$; $R_\infty = 2.5 \times 10^4$ per ft (8.2×10^4 per m).

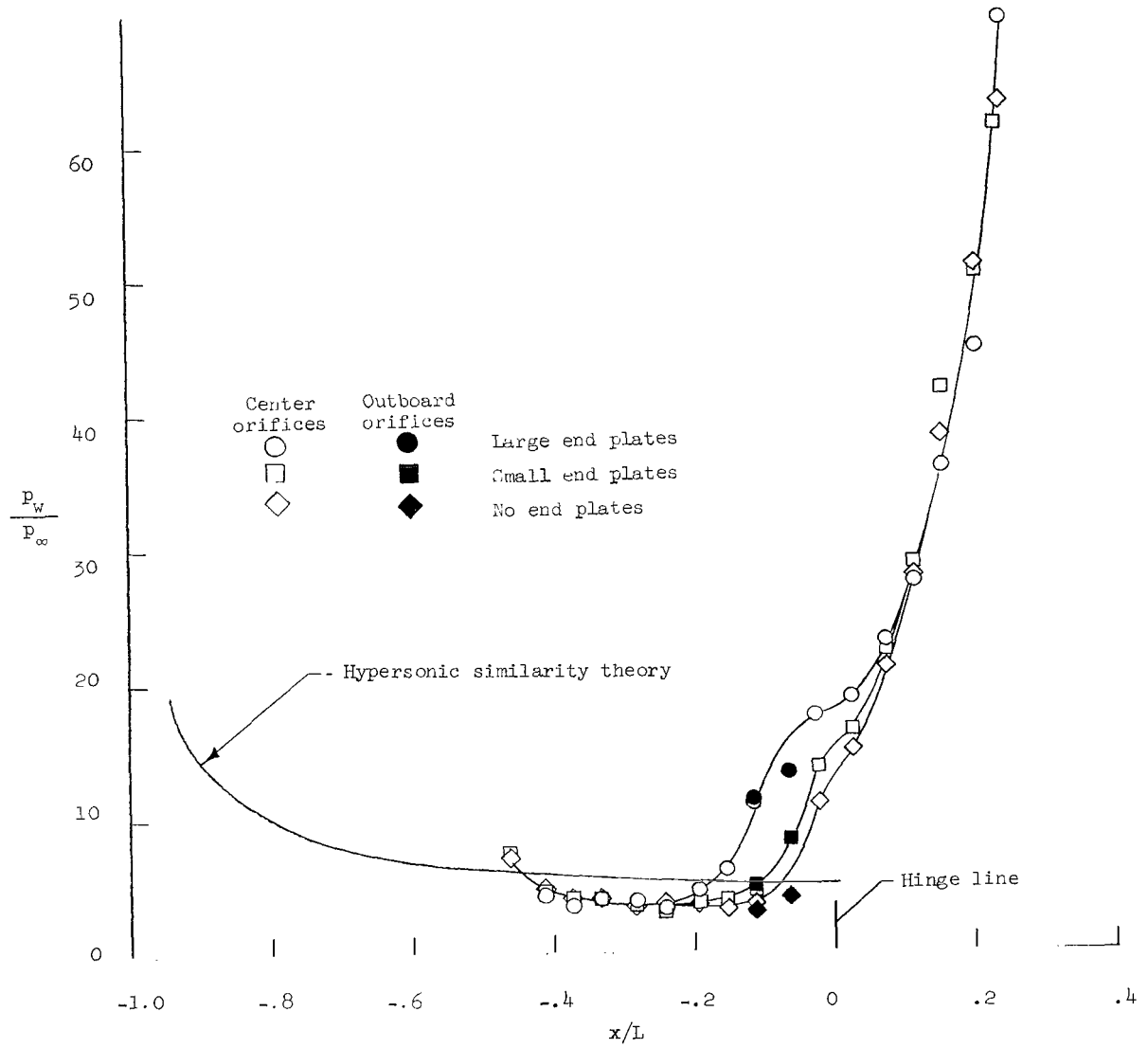

(b) Sharp leading edge.

Figure 5.- Concluded.

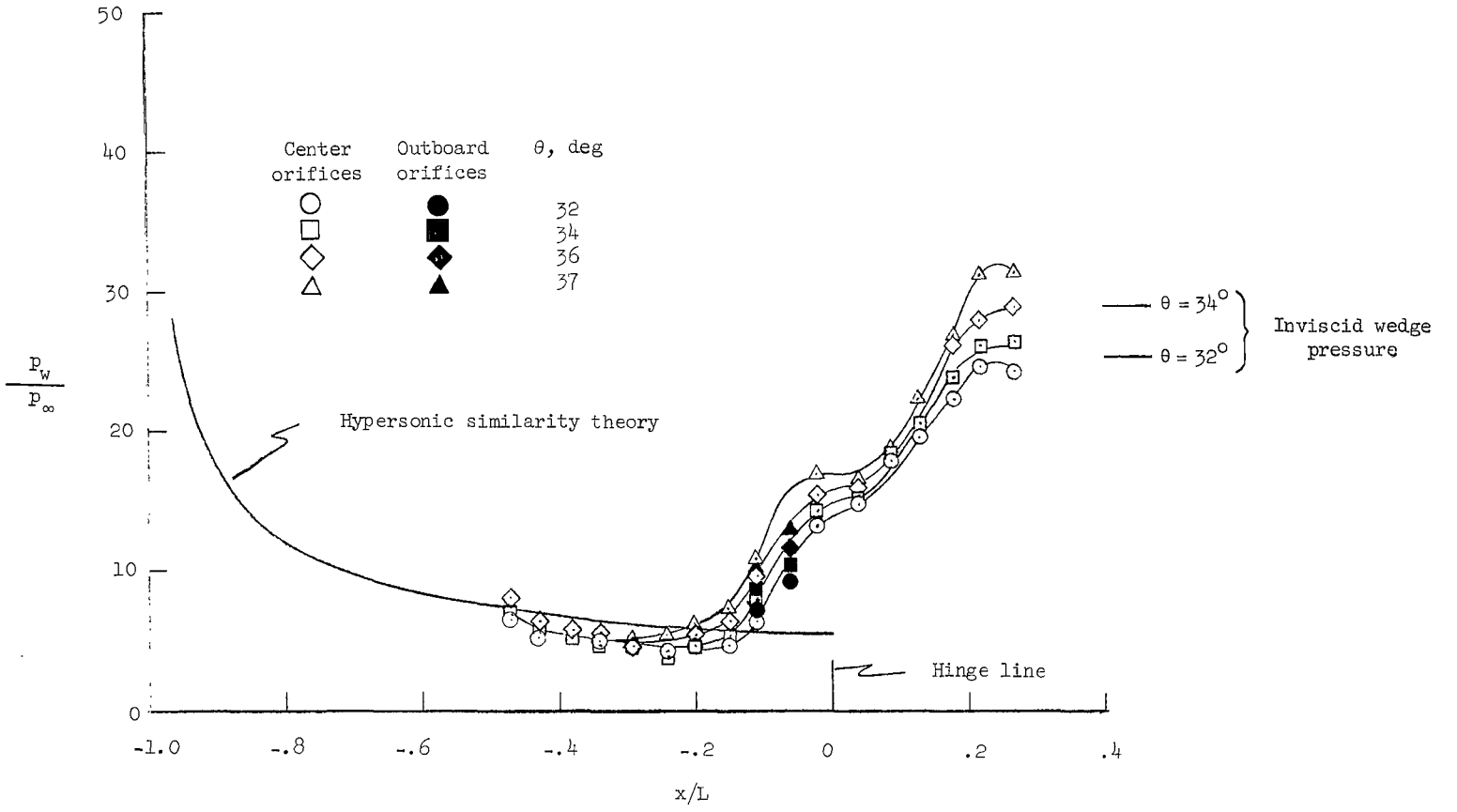

(a) Blunt leading edge.

Figure 6.- Effect of flap angle on pressure distribution with large end plates. $M_\infty = 14.5$; $R_\infty = 2.5 \times 10^4$ per ft (8.2×10^4 per m).

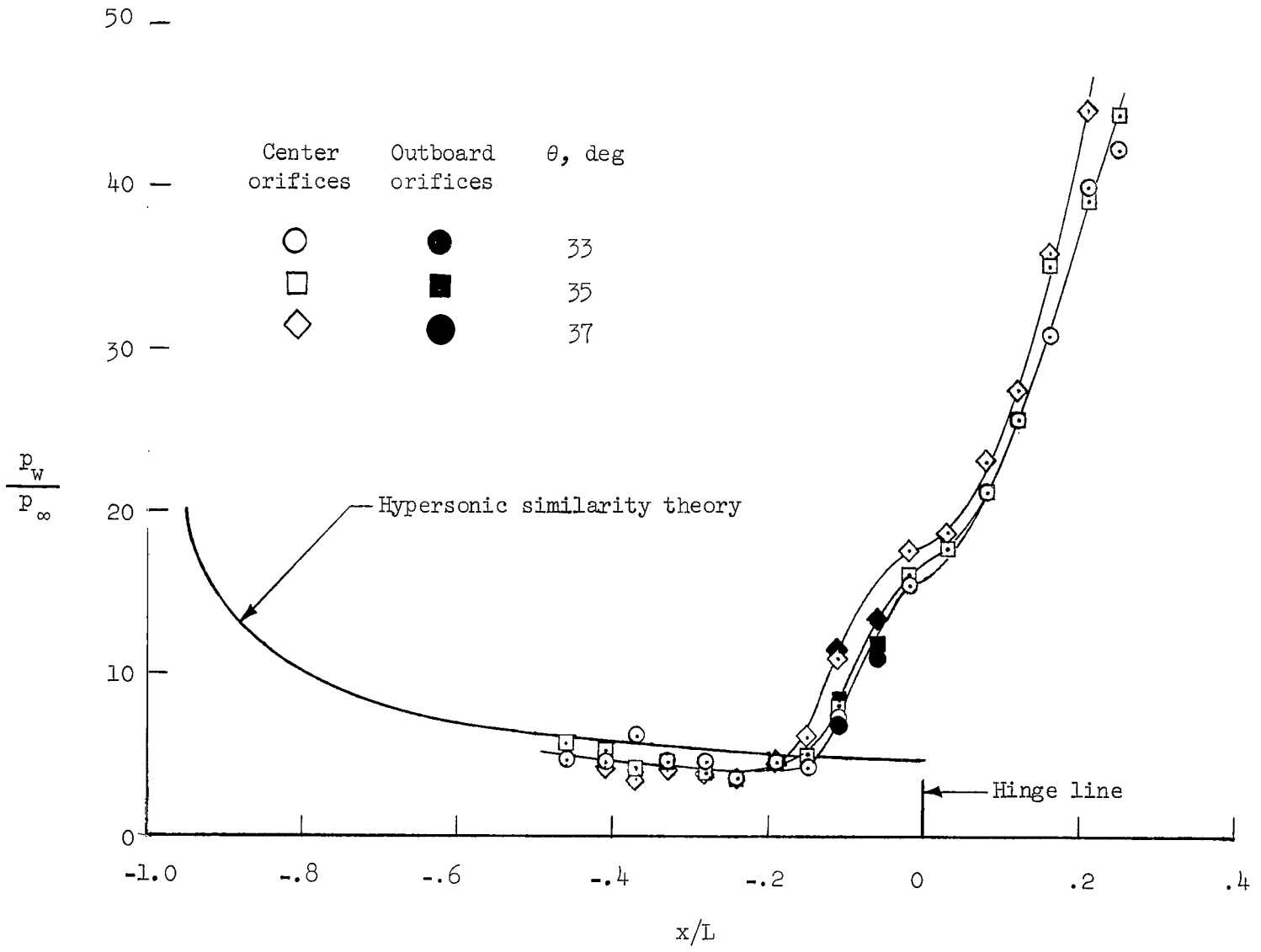

(b) Sharp leading edge.

Figure 6.- Concluded.

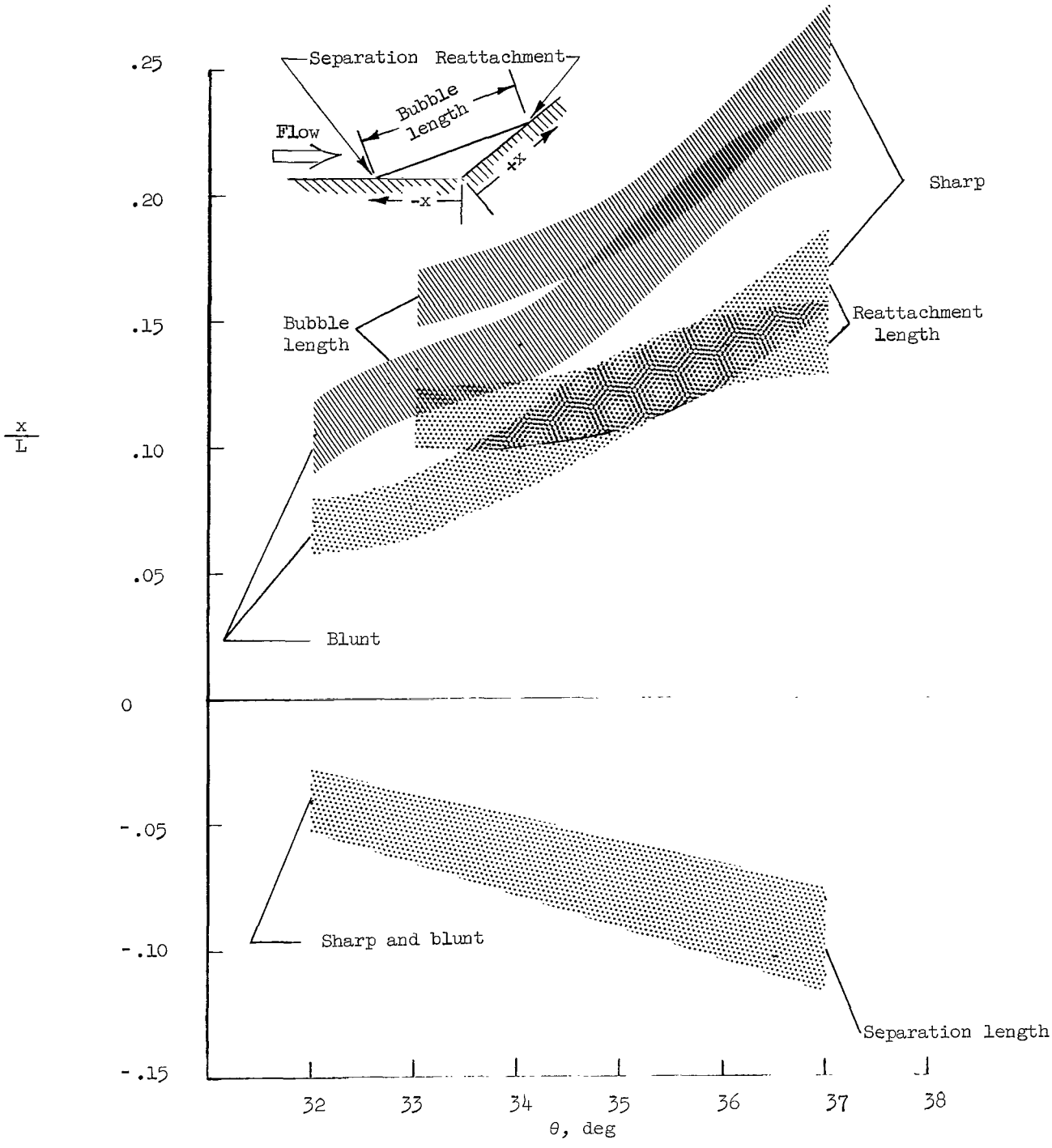

Figure 7.- Effect of flap angle on separation.

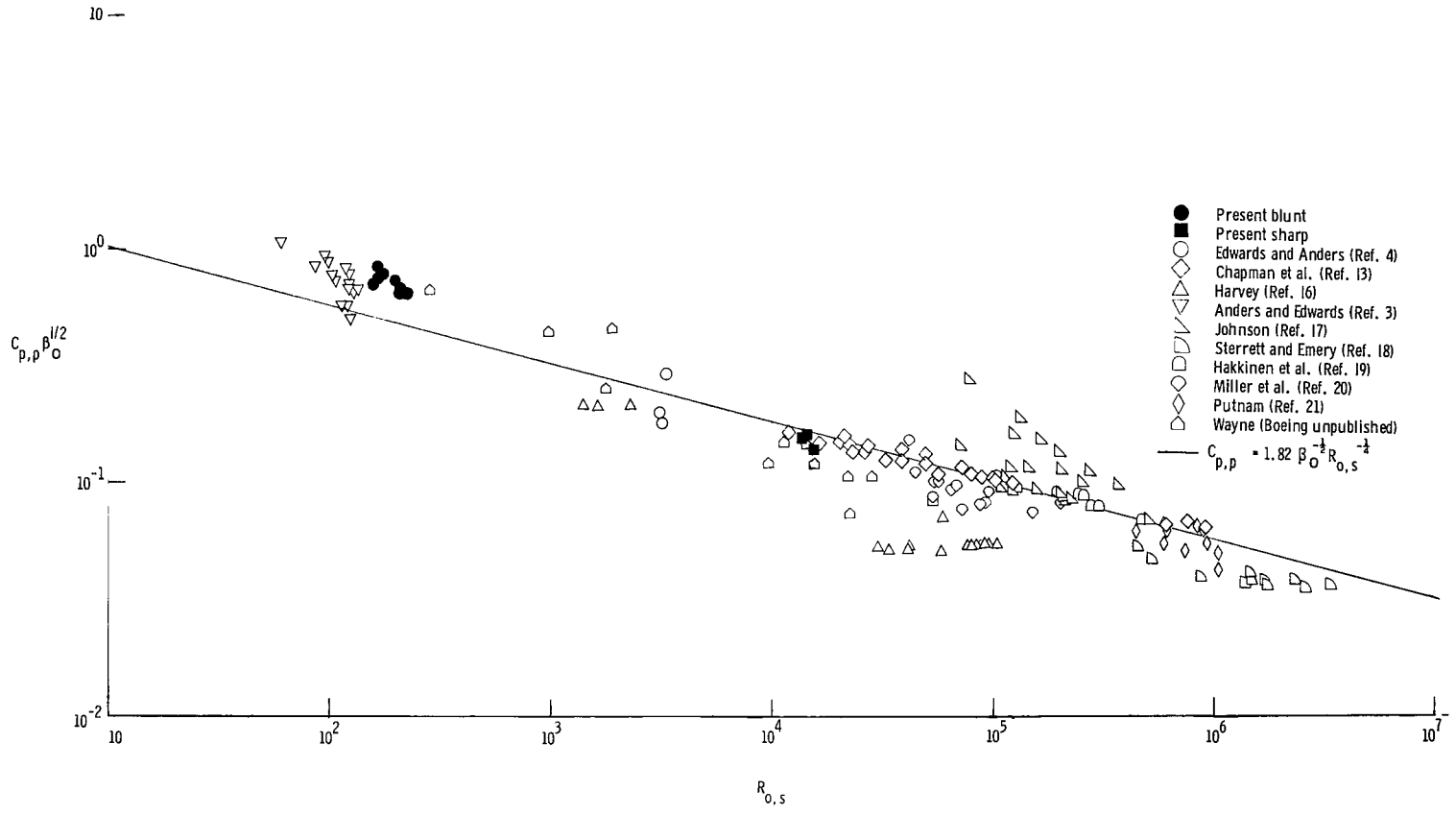

Figure 8.- Plateau-pressure-coefficient correlation with Reynolds number.

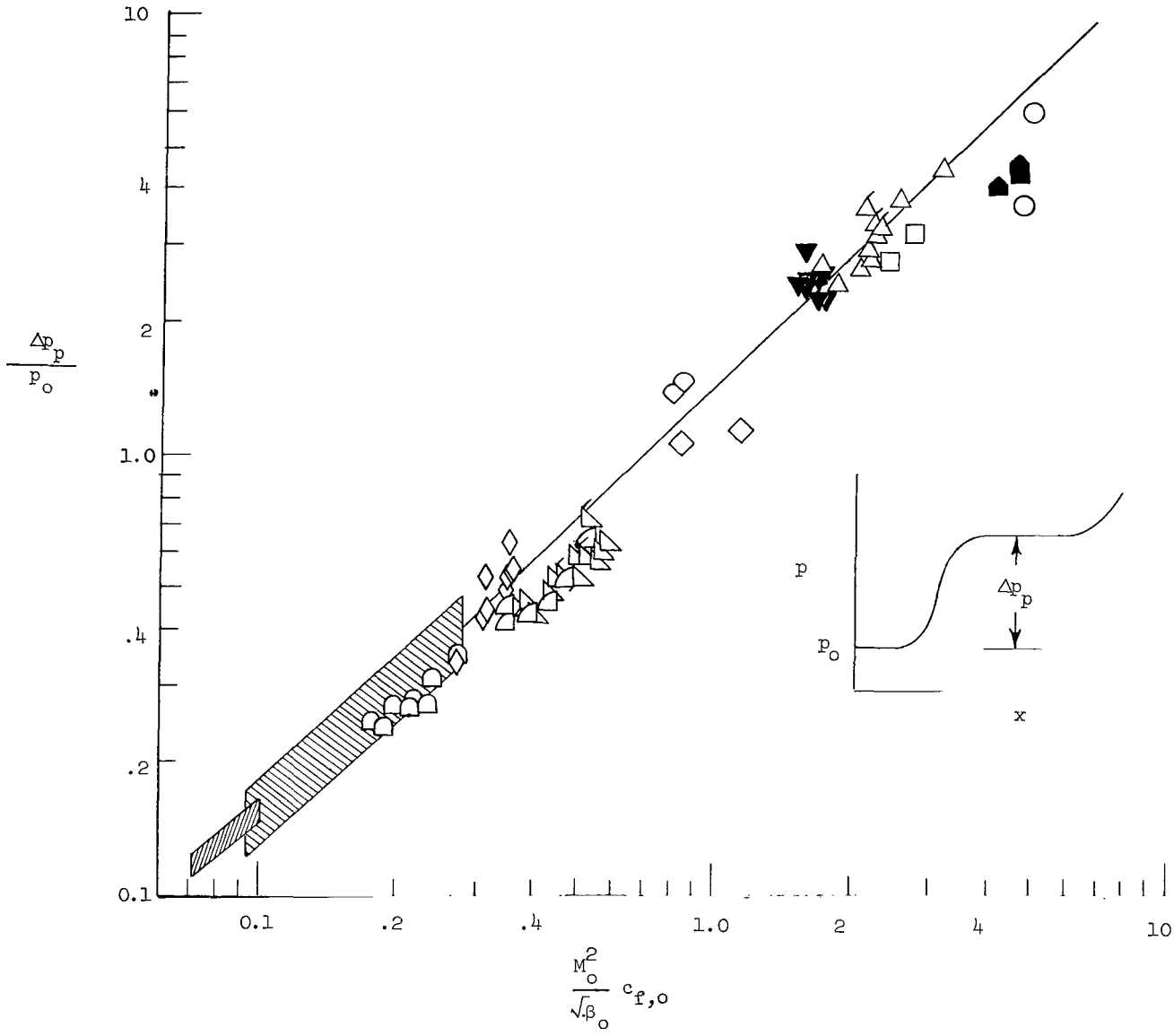

(a) Comparison of present data with previous data.

Figure 9.- Plateau-pressure correlation.

	M_o	M_∞	T_t	T_w	Source
Wedge corner (Sharp L.E.) ▲	12	14.5	6300^o R (3500^o K)	540^o R (300^o K)	Present data
Wedge corner (Blunt L.E.) ▼	3				
Wedge corner ○	17	15.1	4000^o R (2222^o K)	550^o R (306^o K)	Reference 23
Wedge corner □	13				
Wedge corner ◇	5.5				
Wedge corner △	13.3	15.1	5800^o R (3222^o K)	550^o R (306^o K)	Reference 20
Step corner △					
Wedge corner ◺	7.1, 8.1	8.1	1510^o R (839^o K)	T_{aw}	Goldberg and Emery unpublished data
Step corner ◸					
Curved corner ◺					
Wedge corner ◿	5.9, 6.6	6.1	860^o R (478^o K)	T_{aw}	Reference 18
Wedge corner ∩	4.7	4.7	610^o R (339^o K)	T_{aw}	Reference 18
▨	2	2	550^o R (306^o K)	T_{aw}	Reference 19
▨	2.3	2.3	550^o R (306^o K)	T_{aw}	Reference 13
Wedge corner ◇	9.5	10	1560^o R (867^o K)	550^o R (306^o K)	Reference 22
Wedge corner ◇	3.2				

(b) Key to data.

Figure 9.- Concluded.

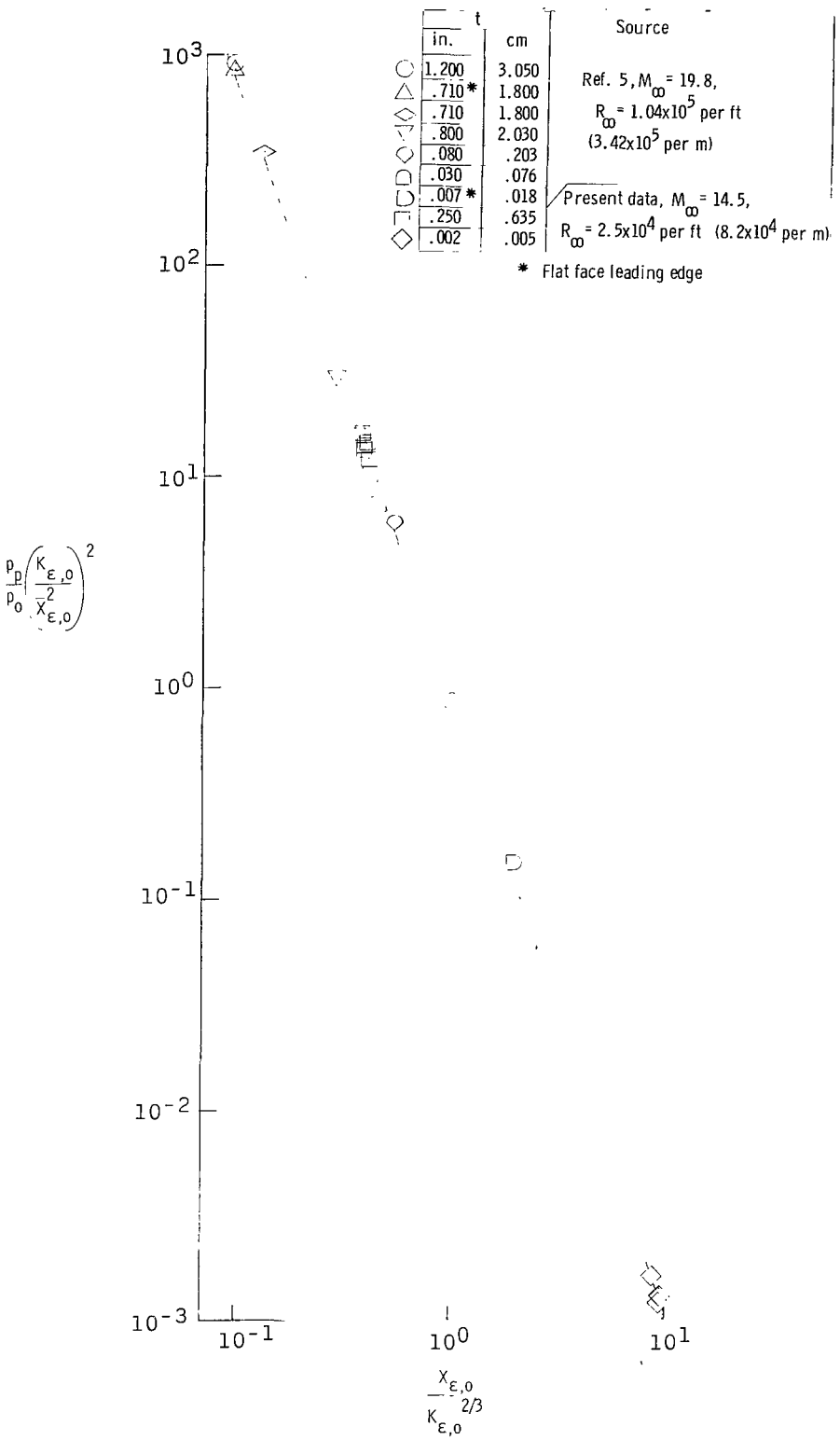

Figure 10.- Correlation of laminar plateau pressure with combined bluntness—viscous-interaction parameter.

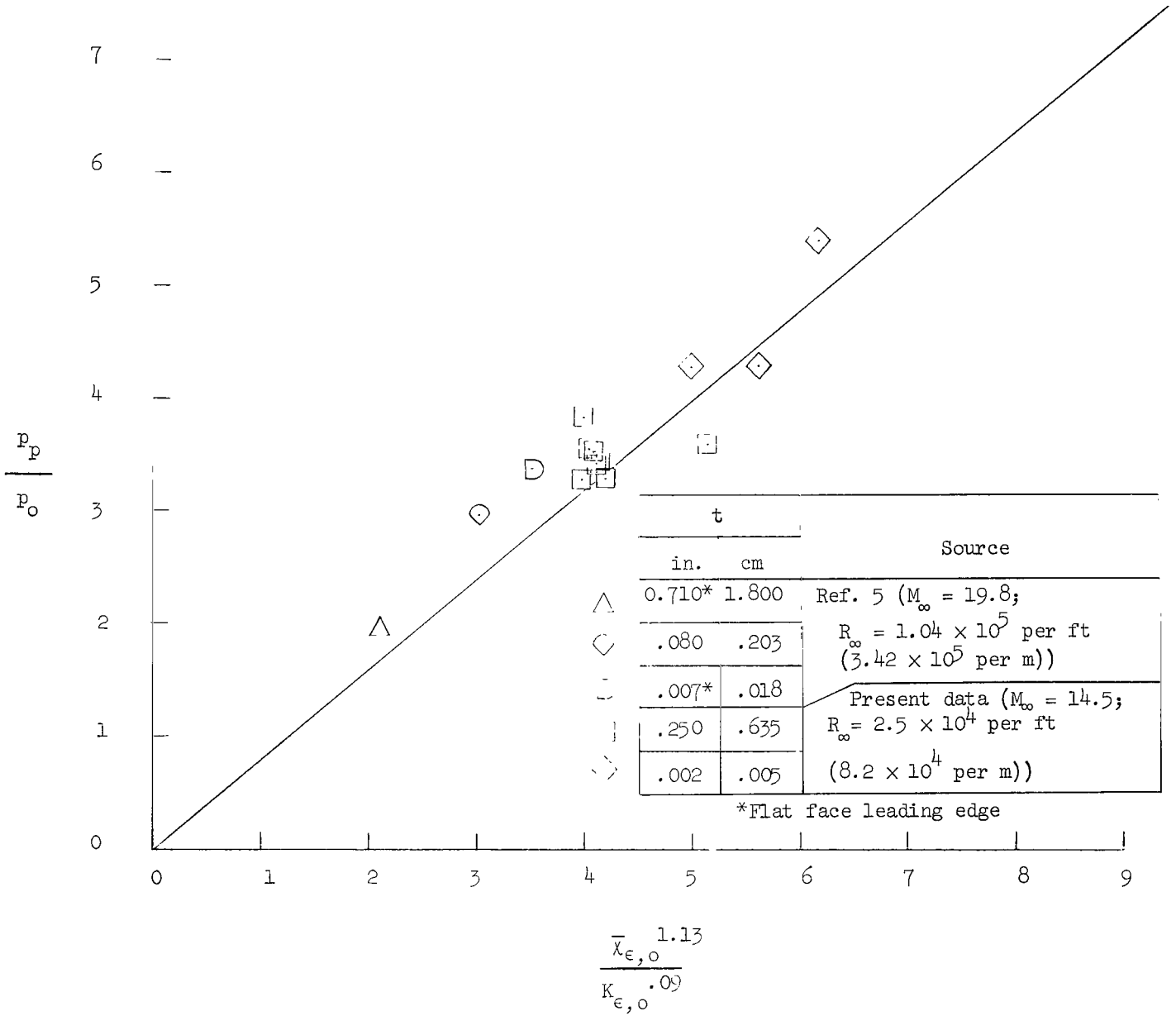

Figure 11.- Modified correlation of laminar plateau pressure with combined bluntness—viscous-interaction parameter.

"The aeronautical and space activities of the United States shall be conducted so as to contribute . . . to the expansion of human knowledge of phenomena in the atmosphere and space. The Administration shall provide for the widest practicable and appropriate dissemination of information concerning its activities and the results thereof."

—NATIONAL AERONAUTICS AND SPACE ACT OF 1958

NASA SCIENTIFIC AND TECHNICAL PUBLICATIONS

TECHNICAL REPORTS: Scientific and technical information considered important, complete, and a lasting contribution to existing knowledge.

TECHNICAL NOTES: Information less broad in scope but nevertheless of importance as a contribution to existing knowledge.

TECHNICAL MEMORANDUMS: Information receiving limited distribution because of preliminary data, security classification, or other reasons.

CONTRACTOR REPORTS: Scientific and technical information generated under a NASA contract or grant and considered an important contribution to existing knowledge.

TECHNICAL TRANSLATIONS: Information published in a foreign language considered to merit NASA distribution in English.

SPECIAL PUBLICATIONS: Information derived from or of value to NASA activities. Publications include conference proceedings, monographs, data compilations, handbooks, sourcebooks, and special bibliographies.

TECHNOLOGY UTILIZATION PUBLICATIONS: Information on technology used by NASA that may be of particular interest in commercial and other non-aerospace applications. Publications include Tech Briefs, Technology Utilization Reports and Notes, and Technology Surveys.

Details on the availability of these publications may be obtained from:

SCIENTIFIC AND TECHNICAL INFORMATION DIVISION

NATIONAL AERONAUTICS AND SPACE ADMINISTRATION

Washington, D.C. 20546